Conference Proceedings

Quantum Sensing Linz 2026

QSL26

20 May 2026

Linz, Austria

RECENDT and JKU
https://www.recendt.at

Imprint

Quantum Sensing Linz 2026 – Conference Proceedings

Dates:	20 May 2026
Venue:	Linz, Austria
Organizer:	RECENDT and JKU
Scientific committee:	Ivan Zorin, Paul Gattinger, and Peter Burgholzer
Website:	https://www.recendt.at
Contact:	ivan.zorin@recendt.at and robert.holzer@recendt.at
Compiled:	2026-05-20
Editor of the Proceedings:	Ivan Zorin
Copyright:	Copyright of individual contributions remains with the respective authors
License:	This volume is distributed under CC BY 4.0, unless otherwise stated
DOI:	10.5281/zenodo.20171447

The contributions in this volume are reproduced from author-provided files. They were submitted for inclusion in the QSL26 conference proceedings and reviewed by the Scientific Committee. The scientific content, figures, references, and formatting remain the responsibility of the respective authors.

RECENDT
RESEARCH CENTER NON DESTRUCTIVE TESTING

JKU
JOHANNES KEPLER
UNIVERSITY LINZ

General Information

Conference venue

Wednesday, 20 May 2026, 12:30–20:00 local time (CEST), hosted by RECENDT and JKU Linz. JKU Event Hall, Altenberger Straße 69, 4040 Linz, Austria.

Scientific Program

The program opens with a welcome and opening speech by Vice-Rector Alberta Bonanni (JKU Linz), Peter Burgholzer (CEO RECENDT), and Ivan Zorin (Head of Quantum Sensing, RECENDT). The core section is represented by invited talks that cover a broad range of current directions in quantum sensing and quantum-enabled high-precision metrology:

Speaker	**Title of the talk**	**Affiliation**
Thorsten Schumm	From atomic to nuclear clocks	TU Wien
Stefan Frick	Quantum Rangefinding	University of Innsbruck
Marlon Placke	Hyperspectral imaging with undetected photons in the mid-IR	Humboldt-Universität zu Berlin
Paul Gattinger	Scanless quantum Fourier transform infrared spectroscopy and chemical mapping	RECENDT
Andreas Schell	Measurement and sensing of and with Quantum Emitters	JKU Linz
Xiaoxun Chen	Optical Widefield Magnetic Resonance Microscopy Using Quantum Sensors in Diamond	Technical University of Munich
Peter Koss	A high resolution and high sensitivity magnetic field camera based on an optically pumped magnetometer	Fraunhofer IPM
Felix Müller	Integrated cavities for next generation quantum photonics and quantum sensors	IQOQI-Vienna

A poster session complements the invited program and provides space for contributed research on quantum sensing and quantum technology. Each poster contribution is introduced by a short flash presentation with one slide, followed by discussion during the poster session. The submitted conference contributions are collected in this volume.
Coffee breaks and informal networking intervals are included between scientific sessions to facilitate discussions among participants, speakers, poster presenters, and industry representatives. In addition, the program is connected to the meeting of the Photonics Austria “Quantum Technology” Working Group (www.photonics-austria.at), offering further opportunities for scientific exchange and networking before the main conference program.

Aim and Scope

Quantum sensing has gained significant momentum over the past decade, establishing itself as a promising alternative to classical instrumentation in terms of sensitivity, cost, and performance. QSL26 – Quantum Sensing Conference Linz 2026 aims to bridge the gap between fundamental quantum physics and applied industrial research, with a particular focus on translating quantum-enabled measurement techniques from the laboratory into practical and industrial applications.

The conference covers a broad range of topics, spanning next-generation quantum photonics for applied metrology, nonlinear interferometry and sensing with undetected photons, quantum magnetometry (NV-center diamond sensors and optically pumped magnetometers), as well as advances in atomic and nuclear clocks. In addition, enabling technologies such as photonic integration, advanced nonlinear optics, and meta-optics are within the scope of QSL26.

The event aims to drive the development of competitive and robust quantum sensors capable of surpassing the limitations of classical metrology. QSL26 promotes exchange between research and industry, bringing together the international research community and industry leaders to foster collaboration and accelerate progress at the interface of fundamental science and practical application.

Contact: office@recendt.at

Contents

Imprint i

General Information ii
Scientific Program ii
Aim and Scope iii

Contributions 1

1 Characterisation of a legacy SQUID-MEG shielded room for the usage with OPM-MEG systems 2
G. Demarchi and N. Weisz

2 Towards Sub-Nanometer Overlay Metrology with Nanoscale Scattering Markers 4
J. Resl and A. W. Schell

3 Long-Range Distributed Acoustic Sensing using Quantum-Enabled Photon Counting 6
G. Weber et al.

4 Detecting single microwave photons with current biased Josephson junctions 8
F. Meyer et al.

5 Enhanced light-matter interactions for quantum technologies and sensing applications 10
A. Lafferty et al.

6 Potential Contributions of Nanoimprint Lithography for Quantum Technologies 12
M. Mühlberger et al.

7 Enhancing Light-Matter Interactions In Integrated Platforms 14
M. Waheed et al.

8 System-Level Optimization of NV−-Diamond-Based Gyroscopes using Pymond 17
M. Hirsch et al.

9 Sensing and Quantum Sensing with Light-Matter Interaction 19
M. Weber et al.

10 Pymond: a package for system level optimization of solid-state spin based devices 20
E. Sánchez-Ibáñez et al.

11 Sensitivity-enhanced mid-IR OCT with undetected photons for additive ceramic manufacturing 22
M. Conti et al.

Organizers & Partners 25

Contributions

This section contains the submitted conference contributions, reproduced from author-provided extended-abstract manuscripts. All contributions were submitted by the respective authors for inclusion in the QSL26 conference volume and were reviewed by the Scientific Committee. The scientific content, figures, references, and formatting of the individual contributions remain the responsibility of the respective authors.

Characterisation of a legacy SQUID-MEG shielded room for the usage with OPM-MEG systems.

Gianpaolo Demarchi[1,2], Nathan Weisz[1,2]

[1]Department of Psychology and Center for Cognitive Neuroscience, University of Salzburg, Austria

[2]Neuroscience Institute, Christian Doppler University Hospital, Paracelsus Medical University, Salzburg, Austria

gianpaolo.demarchi@plus.ac.at

Abstract

Magnetoencephalography (MEG) is traditionally performed with cryogenic SQUID arrays, which provide millisecond-scale non invasive measurements of neuromagnetic activity, but require expensive helium based infrastructure. Optically pumped magnetometers (OPMs) are a promising non cryogenic alternative: they are wearable and can be positioned close to the scalp or peripheral body sites. We characterized a legacy magnetically shielded room housing an operational SQUID-MEG system and helium liquefaction equipment for OPM-MEG use. The room was divided into twelve $\sim$ 1 m^2 parcels, where empty room recordings were acquired to map residual field and sensor saturation. Residual fields were unexpectedly high, reaching $\sim$ 1000 nT peak to peak with local sensor saturation, particularly near the SQUID dewar. In the current configuration, wearable OPM-MEG recordings are essentially not feasible

Introduction and Background

Magnetoencephalography (MEG) is a non invasive technique for measuring magnetic fields generated by neuronal currents. Conventional MEG systems use multichannel SQUID arrays inside magnetically shielded rooms (MSRs) to record neuromagnetic fields in the 10 fT–1 pT range, roughly 10^{-9} of the Earth's magnetic field [1]. Environmental magnetic noise must therefore be strongly attenuated.

Optically pumped magnetometer (OPM) MEG has emerged as an alternative to SQUID-MEG. OPMs are cheaper, do not require cryogenic cooling, and enable flexible/wearable sensor arrays positioned close to the scalp [2]. The modular nature of OPM arrays also enables hybrid and peripheral biomagnetic applications, including concurrent brain and spinal recordings [3] and wearable hyperscanning [4]. Such applications are attractive for centers already equipped with SQUID-MEG, but require careful characterization of the magnetic environment alreadty present, since OPMs are highly sensitive to residual magnetic fields, and movement through non zero fields can generate artefacts or saturate the sensors. Here, we characterized our existing SQUID-MEG shielded room using a 28 sensor / 56 channel FieldLine OPM-MEG system to assess whether combined SQUID/OPM operation is feasible, without additional field compensation.

Methods / Experiment

The measurements were performed inside a magnetically shielded room (MSR; Vacuumschmelze VACOSHIELD). The OPM system consisted of 28 dual axis sensors (56 channels; FieldLine Inc., Boulder, USA) operated in closed loop mode, with a declared sensitivity below 15 $fT/\sqrt{Hz}$, dynamic range of $\pm$150 nT, and bandwidth from DC to 150 Hz, in the closed loop regime. The system was installed in our existing MSR, which also houses a conventional SQUID-MEG system and helium liquefaction unit (MEGIN Triux, MEGIN Oy, Helsinki, Finland).

The measurement area was divided into twelve parcels of approximately 1 m^2. At each location, the array was placed on a non magnetic support and 1 minute empty room recordings were acquired. For each parcel, we extracted the maximum peak to peak signal across channels and the number of saturated sensors (Fig. 1).

Results and Discussion

The residual magnetic field inside the room was substantially higher than expected, with peak to peak values exceeding 1000 nT in some positions and frequent sensor saturation. The spatial pattern suggested that the dominant contribution originated from the existing SQUID-MEG infrastructure, particularly the dewar hosting

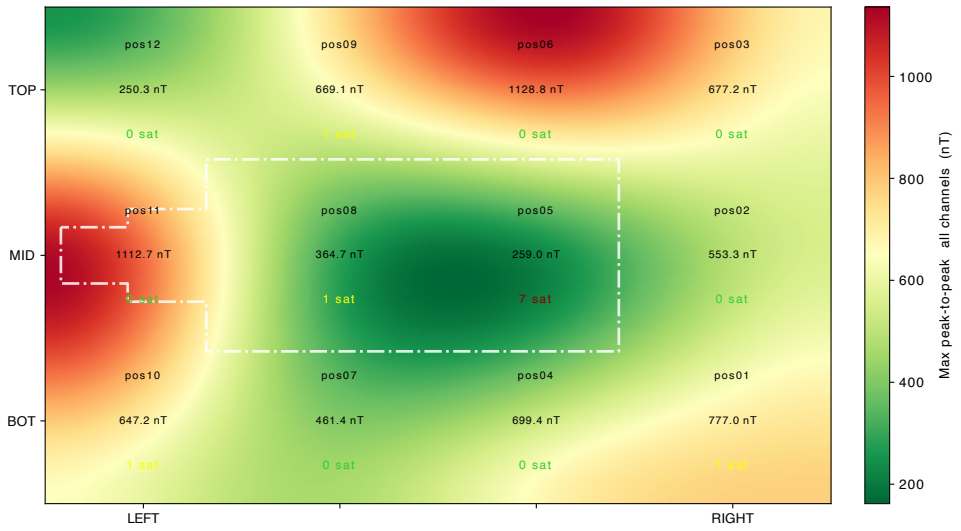


Figure 1: Spatial map of OPM operating conditions inside the legacy SQUID-MEG shielded room. The room was divided into twelve parcels of approximately 1 m^2. For each parcel, the value shown in black indicates the maximum peak-to-peak magnetic signal across all 56 OPM channels. Coloured text indicates the number of saturated sensors. The largest peak-to-peak values, without saturation, occurred near positions 06 and 11, exceeding 1000 nT. The white dash-dotted outline shows the approximate SQUID-MEG position. The existing MSR contains residual fields incompatible with non fixed OPM-MEG arrays.

the helium liquefaction hardware. Although several measured values exceeded the nominal ±150 nT dynamic range of the FieldLine sensors, the system remained mostly operational, indicating greater robustness than anticipated. However, no region of the room approached the low remnant field levels (few nT) typically required for "free moving" OPM-MEG experiments. OPM-optimised environment reported in the literature use strict field nulling, since motion through non-zero background fields can mask brain activity and saturate OPM outputs.

Conclusion

In the current configuration, our legacy SQUID-MEG shielded room is not suitable for reliable OPM-MEG recordings of brain activity. The limiting factor is not intrinsic OPM sensitivity, but the magnetic operating environment: residual fields associated with the SQUID-MEG/cold-head infrastructure push the OPM array outside a usable operating regime and make motion-induced artefacts unavoidable.

References

[1] Matti Hämäläinen, Riitta Hari, Risto J. Ilmoniemi, Jukka Knuutila, and Olli V. Lounasmaa. Magnetoencephalography: theory, instrumentation, and applications to noninvasive studies of the working human brain. *Reviews of Modern Physics*, 65(2):413–497, April 1993. ISSN 0034-6861. doi: 10.1103/RevModPhys.65.413. URL `https://link.aps.org/doi/10.1103/RevModPhys.65.413`.

[2] Matthew J. Brookes, James Leggett, Matthew Rea, Rebecca M. Hill, Niall Holmes, Elena Boto, and Richard Bowtell. Magnetoencephalography with optically pumped magnetometers: the next generation of functional neuroimaging. *Trends in Neurosciences*, 45(8):621–634, August 2022. ISSN 0166-2236. doi: 10.1016/j.tins.2022.05.008. URL `https://doi.org/10.1016/j.tins.2022.05.008`.

[3] Luke C. Mardell, Matthew E. Spedden, George C. O'Neill, Timothy M. Tierney, Niall Holmes, Richard Bowtell, and Matthew J. Brookes. Concurrent spinal and brain imaging with optically pumped magnetometers. *Journal of Neuroscience Methods*, 406:110131, July 2024. ISSN 0165-0270. doi: 10.1016/j.jneumeth.2024.110131. URL `https://doi.org/10.1016/j.jneumeth.2024.110131`.

[4] Niall Holmes, Matthew Rea, Rebecca M. Hill, James Leggett, Elena Boto, Richard Bowtell, and Matthew J. Brookes. Naturalistic hyperscanning with wearable magnetoencephalography. *Sensors*, 23(12):5454, June 2023. ISSN 1424-8220. doi: 10.3390/s23125454. URL `https://doi.org/10.3390/s23125454`.

Towards Sub-Nanometer Overlay Metrology with Nanoscale Scattering Markers

Josef Resl[1], Andreas W. Schell[1]

[1]Institute of Semiconductor and Solid State Physics, Johannes Kepler University Linz, Linz, Austria

josef.resl@jku.at

Abstract

Overlay metrology requires measuring relative marker positions far below the optical resolution limit. We investigate balanced optical scattering as a route toward sub-nanometer overlay readout with nanoscale lithographic markers. A focused 635 nm laser is scanned across line structures while a four-quadrant detector records transmitted and scattered light. Repeated scans of a 200 nm line target show that the raw position signal is dominated by open-loop piezo creep, giving about 35 nm standard deviation. After drift correction and removal of slow laser background variations, the reconstructed scattering signature is much more stable: a symmetry-center estimator gives 0.46 nm standard deviation over ten scans. This does not yet prove absolute sub-nanometer overlay accuracy, but shows that the optical signal contains sub-nanometer marker-position information. We next build a calibrated uncertainty budget combining drift, detector noise, reconstruction error and scattering models.

Motivation

Measuring relative marker positions below the optical resolution limit is a recurring problem in nanofabrication, overlay metrology and compact optical sensing. Balanced optical scattering (BOS) addresses this by using small lithographic structures as scattering markers rather than as objects to be imaged [1]. A focused beam is scanned across the marker, and the marker position is inferred from the symmetry or zero crossing of the detector response. In the ideal case, this converts a small geometric displacement into a very sensitive balance signal.

The project goal is not only to detect small structures, but to turn their scattering signature into a defensible position measurement. This requires separating how precisely the optical signal can locate the feature from what is added by stage drift, detector background, calibration and imperfect scattering simulations. The current work combines repeated line-scan measurements, drift-robust reconstruction and electromagnetic modelling.

Measurement Principle

In the experiment, a fiber-coupled 635 nm laser is focused onto lithographic markers on glass. The sample is moved by a piezo scanner, and transmitted light is recorded on a four-quadrant detector, giving SUM and differential channels. A line-like scatterer produces a spatially structured detector response. Its position can be estimated either from the zero crossing of an antisymmetric component or from a fitted symmetry center of the reconstructed profile.

To reduce sensitivity to slow baseline drift, the position scan is combined with a small sinusoidal dither, $x(t) = X(t) + a\cos(\omega_m t + \phi)$. The nonzero modulation harmonics contain local shape information about the scattering profile, while the DC channel contains the drift-sensitive local mean. Because the position is modulated as a cosine, temporal harmonics can be mapped onto Chebyshev polynomials in position space. This preserves the marker signature while suppressing slow background fluctuations.

Repeatability Result

The most recent repeatability test used ten repeated scans of a 200 nm line. The raw scan positions are not yet stable: the fitted symmetry-center position has a standard deviation of about 35 nm, and the alignment shifts show clear open-loop piezo creep. This is currently the dominant instrumental limitation.

After positional alignment of the repeated profiles and high-pass removal of slow background fluctuations, the line signature itself is highly repeatable. The fitted symmetry-center estimator gives 0.46 nm standard deviation

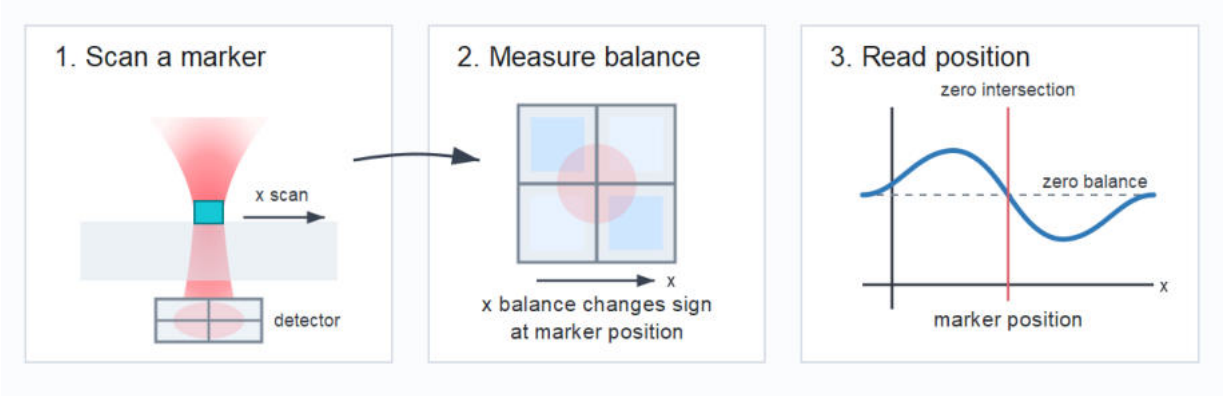


Figure 1: Concept of the readout. A focused beam is scanned over a nanoscale scattering marker, the x-balance changes sign near the marker position, and the zero intersection provides a position estimate.

and 0.15 nm standard error of the mean over ten scans. A simpler zero-crossing estimator gives 1.61 nm standard deviation. The fitted-baseline symmetry estimator is currently the most robust estimator, because it is less sensitive to residual background structure than a pure zero-crossing measurement.

This result should be interpreted carefully. It does not demonstrate that the complete instrument already measures absolute position with sub-nanometer stability in real time. It shows something narrower, but important: once slow mechanical drift, unwanted vibrations and background drift are corrected, the optical scattering profile contains sub-nanometer position information. The next question is how much of the raw scatter can be removed by better hardware and calibration, and how much must remain in the uncertainty budget.

Forward Model and Uncertainty

Electromagnetic modelling connects marker geometry to the measured detector response. The discrete dipole approximation (DDA) treats arbitrary marker shapes [2], while SMUTHI provides an independent T-matrix solver for scatterers in layered media [3]. Simple benchmark simulations reproduce analytical Rayleigh scattering; for markers on a substrate, agreement between DDA and SMUTHI is typically at the few-percent level and becomes more demanding for asymmetric geometries.

The intended deliverable is an uncertainty budget for marker position and, ultimately, overlay displacement. It will separate scanner drift and calibration, detector and laser noise, background subtraction, reconstruction uncertainty and model error. This distinction is essential: sub-nanometer repeatability after correction is promising, but a useful sensor must report when and why such precision is physically meaningful. The present results mark a transition from proof-of-signal toward quantitative overlay metrology with nanoscale scattering markers.

References

[1] Andreas Schell. Verfahren zur Detektion von Positionsabweichungen. Austrian patent AT527414B1; publication version AT527414A4, 2025. Published 15 February 2025; applicant: Universität Linz; inventor: Andreas Schell. Filing number A 50017/2024, filed 16 January 2024.

[2] Bruce T. Draine and Piotr J. Flatau. Discrete-dipole approximation for scattering calculations. *Journal of the Optical Society of America A*, 11(4):1491–1499, 1994. doi: 10.1364/JOSAA.11.001491.

[3] Amos Egel, Krzysztof M. Czajkowski, Dominik Theobald, Konstantin Ladutenko, Alexey S. Kuznetsov, and Lorenzo Pattelli. SMUTHI: A python package for the simulation of light scattering by multiple particles near or between planar interfaces. *Journal of Quantitative Spectroscopy and Radiative Transfer*, 273:107846, 2021. doi: 10.1016/j.jqsrt.2021.107846.

Long-Range Distributed Acoustic Sensing using Quantum-Enabled Photon Counting

Guilherme H. Weber[1,2], Yannik Schick[1], Cicero Martelli[2], Daniel R. Pipa[2], Oliver Lang[3], Thomas Fromherz[3], Moritz Brehm[3], Marco Da Silva[1]

[1]Institute of Measurement Technology, Johannes Kepler University Linz, Austria

[2]Graduate Program in Electrical and Computer Engineering, Federal University of Technology - Parana, Curitiba, Brazil

[3]Institute of Semiconductor and Solid State Physics, Johannes Kepler University Linz, Austria

marco.dasilva@jku.at

Abstract

Conventional Distributed Acoustic Sensing (DAS) utilizes phase-sensitive optical time-domain reflectometry to transform optical fibers into long-range vibration sensors. However, electronic receiver noise typically limits the achievable sensing range. In this work, we overcome these constraints by integrating a highly coherent laser source with a Superconducting Nanowire Single-Photon Detector (SNSPD) within a coherent OTDR topology. By operating in a shot-noise-dominated detection regime, our "Q-DAS" architecture enables distributed strain sensing over a link-loss equivalent of 112.5 km. We demonstrate the accurate reconstruction of low-frequency (∼few Hz) vibrations at these loss-equivalent distances. Consequently, the Q-DAS architecture establishes a new benchmark for long-range geophysical and infrastructure monitoring.

Introduction and Background

Distributed Acoustic Sensing (DAS) has become a cornerstone for seismic monitoring, structural health assessment, and submarine cable surveillance due to its high sensitivity and spatially continuous response [1]. However, the sensing range of conventional DAS architectures is fundamentally constrained by the trade-off between optical nonlinear thresholds and the electronic noise floor of traditional photoreceivers. These limitations typically necessitate the use of optical amplifiers or complex configurations for extra-long-range applications.

While Single-Photon Detectors (SPDs) have successfully extended the reach of traditional OTDR systems and enhanced distributed temperature sensing [2], their application to phase-sensitive, dynamic strain measurement remains largely unexplored. This work addresses this gap: we present the first experimental demonstration of coherent distributed strain measurement via single-photon counting, operating in a quantum-enabled readout regime to achieve high-fidelity vibration sensing over a 112.5 km link-loss equivalent.

Methods / Experiment

The Q-DAS architecture (Fig. 1a) utilizes a coherent OTDR topology where nanosecond pulses are launched at a kilohertz repetition rate. As the pulse propagates, it excites a spatial gauge length, generating a Rayleigh backscattered wavefront from the fiber's random scattering centers. This backscattered light travels back to the interrogator, where its interference pattern is mapped to a spatial position via time-of-flight.

In conventional DAS, this interference is recorded as an analog power signal. In the proposed Q-DAS, the SNSPD samples this field at the single-photon level. Each detection event ("click") represents a random draw from a Poissonian probability distribution proportional to the local backscattered intensity. By integrating these events over subsequent pulses, the system reconstructs the interference-driven "speckle" statistics. Dynamic strain is then extracted by tracking phase-induced changes in this speckle pattern, with the SNSPD's high efficiency and low dark-count rate enabling operation at the fundamental shot-noise limit over extreme link-loss budgets.

To validate the system, a 3-minute test was conducted by applying a 1 Hz sinusoidal stimulus at 5 V, 3 V, and 1 V in successive 30 s intervals (inducing strains of approximately 1.14 $\mu\varepsilon$, 682 nε, and 227 nε, respectively), with the stretcher deactivated between sets.

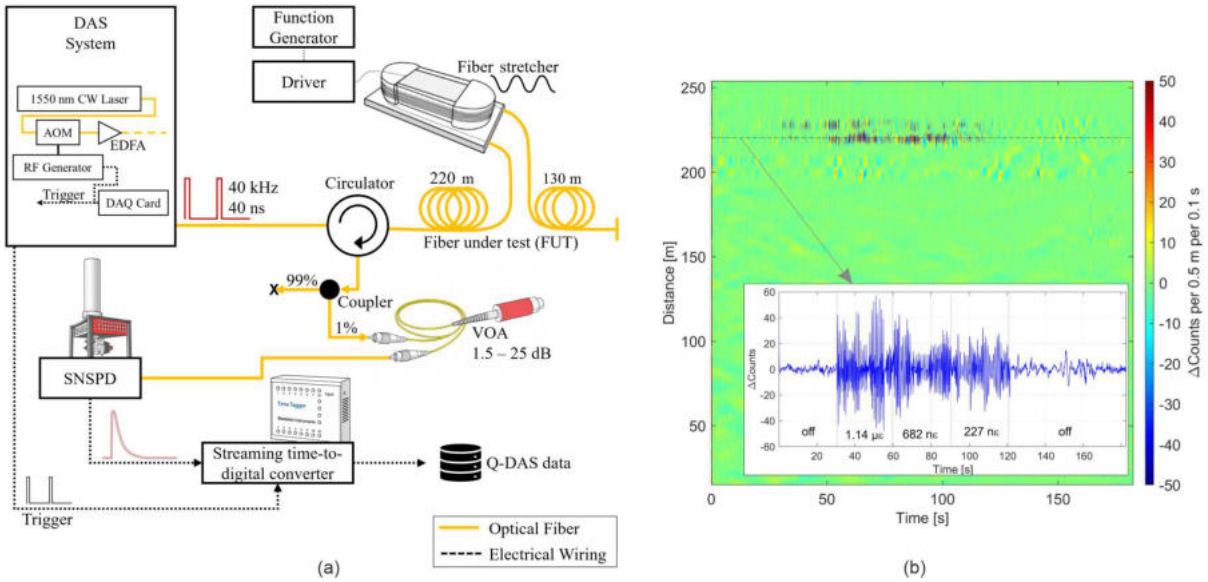


Figure 1: (a) Q-DAS experimental setup. A ϕ-OTDR interrogator and SNSPD are coupled via an optical circulator; a VOA and couplers emulate a 112.5 km link-loss. (b) Space–time map of high-pass filtered photon count variations. The 1 Hz stimulus is localized at ∼220 m. Inset: Reconstructed time-domain signal at the stretcher position, showing the 1 Hz component and three distinct strain amplitudes in successive 30-second intervals between 30 and 120 s.

Results and Discussion

The processed Q-DAS signal (Fig. 1b) was obtained by applying a 0.5 Hz high-pass filter followed by spatial (5 m) and temporal (0.2 s) moving-average filters to the photon-count distribution. The fiber stretcher region at 220 m exhibits peak-to-peak variations of ∼100 photons per bin, while quiescent regions remain below 10 counts, demonstrating a high signal-to-noise ratio (SNR). The 1 Hz stimulus is clearly localized and reconstructed across the 30–120 s test window.

The Q-DAS architecture demonstrates remarkable stability over high-loss channels. Despite an emulated link-loss of 45 dB, the backscattered interference pattern remains clearly resolvable. This high SNR is maintained by the SNSPD's near-zero dark count rate, ensuring that even at the single-photon level, the temporal evolution of the speckle pattern is dominated by the physical strain rather than receiver noise. This capability is critical for extra-long-range applications where backscattered power traditionally falls beneath the thermal noise floor of analog photoreceivers.

Key performance highlights of the Q-DAS demonstration:

- Distributed sensing over an emulated loss budget of 45 dB (equivalent to 112.5 km SMF);
- Detection of strain amplitudes as low as 227 nε at 1 Hz;
- Shot-noise-dominated operation at a ∼650 kcps average count rate;
- Robust vibration localization via single-photon statistics.

Unlike conventional DAS systems, the sensing range is not limited by electronic noise floors; it can be further scaled via higher launch power or adjusted integration times. This work establishes the feasibility of quantum-readout architectures for long-range geophysical and submarine monitoring. Future efforts will focus on detailed characterizaton of sensitivity limits (e.g. based on modelling [3]), explore phase-demodulation to linearize the strain response as wel as real-world deployment on long-haul fiber links.

References

[1] Zuyuan He and Qingwen Liu. Optical fiber distributed acoustic sensors: A review. *Journal of Lightwave Technology*, 39(12):3671–3686, 2021. doi: 10.1109/JLT.2021.3059771.

[2] T. Staffas, F. Troive, and V. Zwiller. Temperature measurements in deployed optical fiber networks using single photon optical time domain reflectometry. *Optics Express*, 31(5):8170–8176, 2023. doi: 10.1364/oe.483404.

[3] G. H. Weber, D. F. Gomes, E. H. Dureck, B. Brusamarello, J. C. C. da Silva, C. Martelli, D. R. Pipa, M. F. da Silva Junior, S. T. de Camargo Junior, and M. J. da Silva. Fundamental DAS sensor numerical model for high- and low-frequency stimuli. *IEEE Sensors Letters*, 9(10):1–4, 2025. doi: 10.1109/LSENS.2025.3610287.

Detecting single microwave photons with current biased Josephson junctions

Felix Meyer[1,2], Alejandro Andrés Juanes[1], Samarth Hawaldar[1] Andrea Trioni[1] Johannes Fink[1]

[1]Institute of Science and Technology Austria, 3400 Klosterneuburg, Austria

[2]Faculty of Physics, University of Vienna, 1090 Vienna, Austria

Johannes.Fink@ist.ac.at

Abstract

We investigate current-biased Josephson junctions (JJ) as single-shot detectors of microwave photons. A DC bias creates a tilted washboard potential with bound states whose tunneling rate to the voltage state is exponentially enhanced by the absorption of a photon. Simulations for a target frequency of 8.9 GHz indicate operation at $I_b/I_c = 84\,\%$ to $85\,\%$ with predicted detection efficiency above $80\,\%$ tunable within a 100 MHz window and with an acceptance bandwidth of ~ 2 MHz. If validated experimentally, this approach will enable single-shot and heralding measurements for quantum sensing and communication.

Introduction and Background

Detecting individual quanta at microwave energies is challenging yet impactful, particularly for single 10 GHz photons (40 µeV). Potential applications include quantum radar, characterization of cosmic microwave radiation, axion dark-matter searches, and single-spin nuclear magnetic resonance spectroscopy. Such capability also supports (heralded) quantum communication and device characterization.

Currently used solutions often rely on amplifiers that also amplify noise and vacuum fluctuations. Current-biased JJs have demonstrated $g^{(2)}$ measurements of thermal cavities [1, 2] and operation with few-photon pulses [3]. To our knowledge, their use as true single-shot, single-photon detectors has not been shown, despite theoretical predictions of efficiencies exceeding 80 % [4, 5]. We plan to show this using a full characterization including quantum efficiency and dark counts.

Working principle

A current-biased JJ switches between a superconducting state with zero DC voltage ($\dot{\phi} = 0$) and a resistive state with a measurable microvolt output ($\dot{\phi} \neq 0$). The bias tilts the cosine potential, creating a local minimum that supports bound states, see figure 1 (a-b). From these states, the phase can quantum-tunnel through the barrier into the continuum. After escape, ϕ evolves in time, producing a finite voltage. Absorption of a photon promotes the system to an excited bound state with a higher tunneling rate. Once tunneled, a finite voltage lays across the JJ yielding a detectable "click" [6].

Chip design

While the tunneling rate from the ground state poses a fundamental dark count limit we try to reduce the other noise sources with a sophisticated chip design, compare figure 1 (c-f). As shown in Fig. 1 (g), an input resonator restricts RF access to the frequencies of interest, while band-stop and low-pass filters on the DC line suppress signal leakage and mitigate bias noise. The detector operates optimally near critical coupling, where the input coupling rate matches the photon-assisted tunneling (switching) rate. Limited in situ tuning is achieved via the bias current which shifts both tunneling rate (dependent on local barrier height) and the resonance frequency.

Results and Discussion

Simulations predict operation at $i = I_b/I_c = 84\,\%$ to $85\,\%$ around 8.9 GHz, providing a 100 MHz operating window within which the efficiency calculated using [5] exceeds $80\,\%$. The intended resonator bandwidth is approximately 2 MHz. Experimental validation is underway.

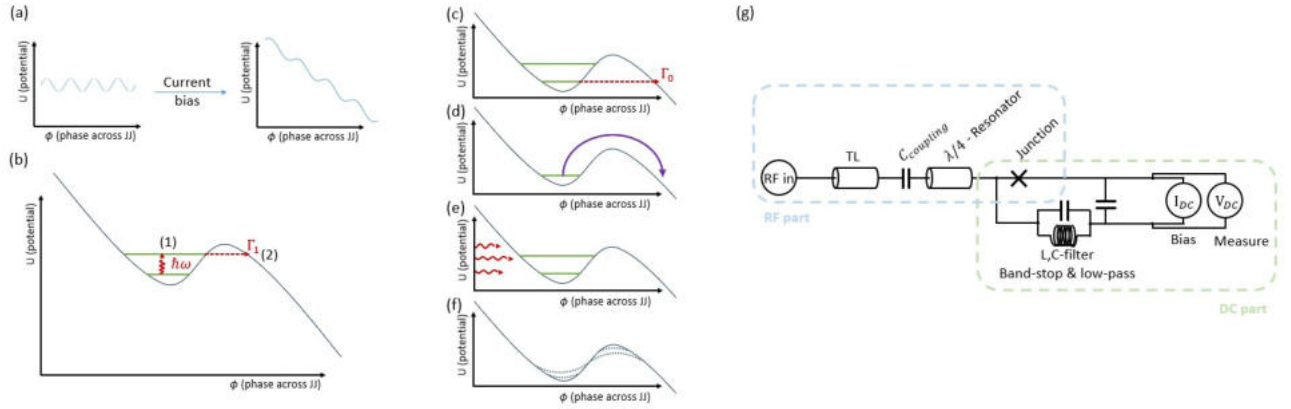


Figure 1: Working principle and noise sources: (a) biasing the JJ tilts the cosine potential of the phase, resulting in local minima for the phase. (b) Zoom into a local minimum that exhibits bound states to illustrate the working principle: An impinging photon excites the junction from the ground to an excited state, which has a higher probability to tunnel. Noise mechanisms include (c) ground-state tunneling, (d) thermal activation (Brownian motion of the phase), (e) thermally occupied background radiation, and (f) bias-current noise that modulates the potential. (g) The chip design combines a DC and RF part.

References

[1] Y.-F. Chen, D. Hover, S. Sendelbach, L. Maurer, S. T. Merkel, E. J. Pritchett, F. K. Wilhelm, and R. McDermott. Microwave photon counter based on josephson junctions. 107(21):217401. doi: 10.1103/PhysRevLett.107.217401. URL https://link.aps.org/doi/10.1103/PhysRevLett.107.217401.

[2] A. L. Pankratov, A. V. Gordeeva, A. V. Chiginev, L. S. Revin, A. V. Blagodatkin, N. Crescini, and L. S. Kuzmin. Detection of single-mode thermal microwave photons using an underdamped josephson junction. 16(1):3457. ISSN 2041-1723. doi: 10.1038/s41467-025-56040-4. URL https://www.nature.com/articles/s41467-025-56040-4.

[3] F. Chiarello, D. Alesini, D. Babusci, C. Barone, M. M Beretta, B. Buonomo, A. D'Elia, D. Di Gioacchino, G. Felici, G. Filatrella, L. G. Foggetta, A. Gallo, C. Gatti, C. Ligi, G. Maccarrone, F. Mattioli, S. Pagano, L. Piersanti, A. Rettaroli, S. Tocci, and G. Torrioli. Investigation of resonant activation in a josephson junction for axion search with microwave single photon detection. 32(4):1–5. ISSN 1558-2515. doi: 10.1109/TASC.2022.3148693. URL https://ieeexplore.ieee.org/document/9705581.

[4] A. Poudel, R. McDermott, and M. G. Vavilov. Quantum efficiency of a microwave photon detector based on a current-biased josephson junction. 86(17):174506. doi: 10.1103/PhysRevB.86.174506. URL https://link.aps.org/doi/10.1103/PhysRevB.86.174506.

[5] M Schöndorf, L C G Govia, M G Vavilov, R McDermott, and F K Wilhelm. Optimizing microwave photodetection: input–output theory. 3(2):024009. ISSN 2058-9565. doi: 10.1088/2058-9565/aaa7f7. URL https://doi.org/10.1088/2058-9565/aaa7f7.

[6] John M. Martinis, Michel H. Devoret, and John Clarke. Energy-level quantization in the zero-voltage state of a current-biased josephson junction. 55(15):1543–1546. doi: 10.1103/PhysRevLett.55.1543. URL https://link.aps.org/doi/10.1103/PhysRevLett.55.1543.

Enhanced light-matter interactions for quantum technologies and sensing applications

Adam Lafferty[1], Raphael Neubacher [1], Helmut Hörner[1], Malaika Waheed [1,2], Ambika Shorny[1], Fritz Steiner[1], Alex Götz[1], Adarsh Prasad[1], Stefan Walser[1], Sarah M. Skoff[1],

[1]Atominstitut, Tu Wien, Stadionallee 2, 1020, Wien

[2]Fachhochschule Wiener Neustadt, University of Applied Sciences, Austria

sarah.skoff@tuwien.ac.at

Abstract

Strong light-matter interactions are important both for quantum networks and for sensing applications. Achieving such coupling has long been a challenge for conventional bulk optical platforms. Recent advances in nanofabrication have opened the door to nanophotonics as a powerful platform for enhancing light matter interaction. This poster shows how different types of nanophotonic platforms can be employed to enhance the interaction between single quantum emitters and a light field. This poster also shows that a strong light matter interaction is crucial in the wider context of environmental sensing, where we have demonstrated that we can detect and identify nanoplastic particles down to sizes of 100nm.

Stable Room Temperature Photon Emitters

Phase 2.0 quantum technologies rely on the development of stable single photon emitters that work under ambient conditions. Hexagonal Boron Nitride (hBN) is a 2D wide bandgap semiconductor that hosts various atomic scale defects that act as optically active centres. These defect states result in bright, stable and spectrally distinct emission of single photons under ambient conditions. hBN's layered structure and chemical robustness make it highly compatible for photonic integration and scalable quantum technologies.

There are several methods of producing hBN. This poster describes the characteristics of hBN made by both CVD (Chemical Vapour Deposition) and LPE (Liquid Phase Epitaxy) and the properties of their quantum emitters[1].

Sensing Platforms to Detect Nanoplastics

Due to limited detection methods, the concentration of nanoplastics in the environment still remains uncertain. Defined as plastic particles smaller than 1 µm, nanoplastics can penetrate biological barriers and have been observed to cross into the brain and placenta. Reliable techniques for their detection and characterisation are therefore essential. Surface-Enhanced Raman Spectroscopy (SERS) offers a promising detection method[2]. Implementation of this technology relies on advances in nanophotonic platform design and fabrication.

Experimental Methods

In both experiments, characterisation is performed using a home-built confocal microscope, though the measurement approach differs depending on the sample. For hexagonal boron nitride (hBN), we are interested in coupling single photon emitters to optical nanophotonic waveguides and cavities. Confocal microscopy enables spatial localisation of individual emitters, followed by spectral characterisation to determine features such as the zero phonon line and phonon sidebands. Additionally, second-order correlation measurements are carried out to verify single-photon emission.

In the case of nanoplastics, plasmonic substrates are employed to enhance detection sensitivity. Confocal scans allow for the localisation of nanoparticles, while plasmonic enhancement enables surface-enhanced Raman spectroscopy (SERS), significantly boosting the inherently weak Raman signal. This facilitates both Raman imaging of the particles and spectral identification..

Results and Discussion

Despite being at room temperature, hBN has a spectrally distinct zero phonon line (ZPL) demonstrating a narrow line width in the visible. hBN has also been confirmed to have high quality single photon characteristics with a clear second order correlation dip below 0.5[1]. One issue with hBN is randomised distribution of emitters, to combat this work has been done to create methods of deterministically localising emitter sites. By growing hBN monolayers via CVD an additional graphene grid mask can be added. This grid will create a deterministic position of emission sites. Where an emitter lines up with a grid hole, the emission will pass through and all other emissions will be quenched by the grid. This method of emitter localisation is highly versatile and compatible with wider nanophotonic devices[3]. Photonic coupling is not only limited to monolayer hBN. By decreasing the diameter of an optical fibre below the wavelength of light that travels through it, evanescent fields in the fibre are excited. If multilayer flakes of hBN are then deposited on top of the fibre the quantum emitters inside the flake are evanescently coupled[1].

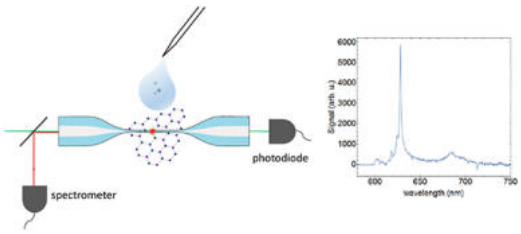


Figure 1: Quantum emitters evanescently to the guided modes of an optical nanofibre.[1].

In order to utilise the effects of plasmonic surface enhancement, samples containing nanoparticles were deposited on top of plasmonic substrates (SERS)[2]. Where a nanoparticle overlaps with a plasmonic hotspot, the Raman signal of the particle is enhanced by up to 3 orders of magnitude. Plasmonic enhancement greatly increases the signal to background ratio and in some cases, makes nanoparticles detectable which would have previously been lost in the background. This was tested by depositing nanoparticles of diameter 800nm and 300nm on both a glass slide and the SERS plasmonic substrate. The 800nm particles were detectable on both the glass and SERS substrates but the Raman signal of the SERS substrate sees an increase of just under 3 orders of magnitude. However, on glass, the 300nm particles are indistinguishable from the background, but when placed on the SERS substrate there is a clear Raman signal. These results can be viewed in figure 2. Future work with this technology involves developing the SERS substrates to further enhance the scattered signal.

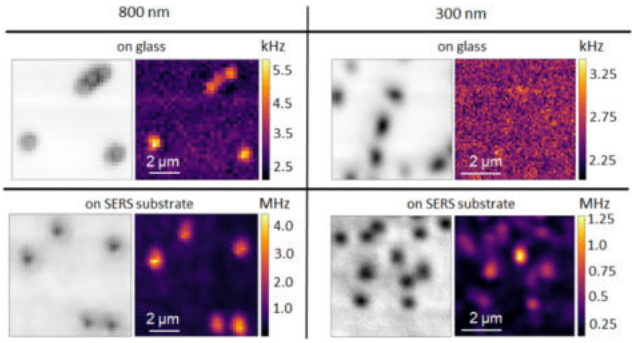


Figure 2: Comparison of 800nm and 300nm nanoparticles on glass and SERS substrate[2].

References

[1] A. Shorny, H. Schauffert, J. C. Stewart, S. Ali, S. Walser, H. Hörner, A. S. Prasad, V. Babenko, Y. Fan, D. Eder, K. S. Thygesen, S. Hofmann, B. C. Bayer, and S. M. Skoff. Properties of quantum emitters in different hbn sample types particularly suited for nanophotonic integration. *Materials for Quantum Technologies*, 2025. URL `https://arxiv.org/abs/2210.11099`.

[2] A. Shorny, F. Steiner, H. Hörner, and S. M. Skoff. Imaging and identification of single nanoplastic particles and agglomerates. *Scientific Reports*, 2023. URL `https://www.nature.com/articles/s41598-023-37290-y`.

[3] J. C. Stewart, Y. Fan, J. S. H. Danial, A. Goetz, A. S. Prasad, O. J. Burton, J. A. Alexander-Webber, S. F. Lee, S. M. Skoff, V. Babenko, and S. Hofmann. Quantum emitter localization in layer-engineered hexagonal boron nitride. *ACS Nano*, 2021. URL `https://pubs.acs.org/doi/10.1021/acsnano.1c04467`.

Potential Contributions of Nanoimprint Lithography for Quantum Technologies

Michael M Mühlberger[1], Sonja Kopp[1], Viktorija Jonaityte[1], Michael J Haslinger[1]

[1]Micro- & Nanofabrication, PROFACTOR GmbH, Steyr-Gleink, Austria

michael.muehlberger@profactor.at

Abstract

Nanoimprint Lithography, as a cost-efficient, high-resolution and versatile nanopatterning technology, provides several solutions for micro- and nanomanufacturing challenges in the field of quantum technologies. This poster will give a short overview and should act as a starting point for further discussion.

Introduction and Background

Nanoimprint Lithography is a replication technology for micro- and nanostructures [1]. It is highly versatile as far as the kind of structures is concerned as well as in terms of materials and applications, which range from life sciences to micro- and metaoptics. In a single process step, complex geometries can be replicated with high fidelity covering a size range from a few nanometers to several 100 micrometers. Figure 1 shows a schematic process flow of a typical nanoimprint process. A master structure (a) (generated by e.g. e-beam lithography, two-photon-polymerization, diamond turning, etc.) is used to replicate a stamp (b,c), which is then pressed into a liquid coating on a substrate (d,e). While still in contact, the liquid is UV-cured (e) and finally the stamp is removed (f), leaving the topography of the master on the substrate.

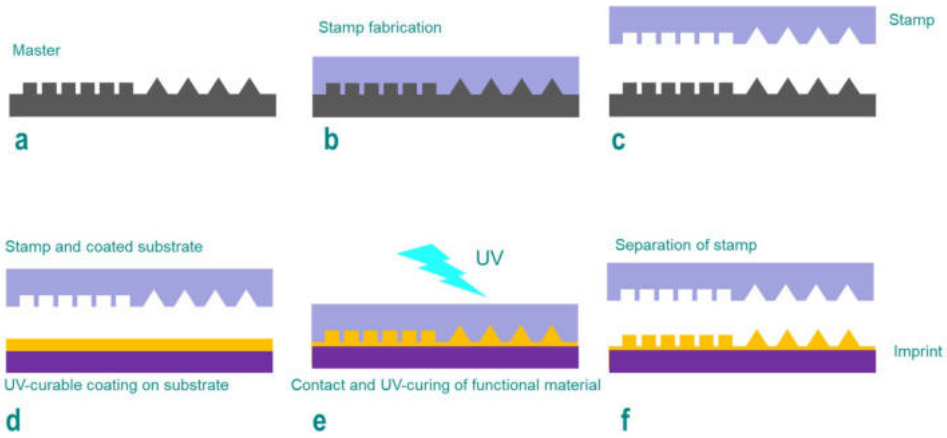


Figure 1: Schematic process flow for a typical nanoimprint process.

Examples

At Profactor, we use various types of nanoimprint processes, on rigid and flexible, as well as on flat and non-flat substrates [2]. To achieve larger patterned areas from a single, small area master step & repeat NIL processes are employed. Figure 2 shows results of such processes, which are available for both nanostructures and microstructures.

Large area replication of such structures is possible using roller-based processes (roll-to-plate NIL), also on non-transparent substrates, up to 30x60cm^2 in size [3]. Typical applications are diffractive optical elements, waveguides, or microlens arrays. Co-packaged optics is an upcoming topic for NIL. An interesting option for nanoimprinting is also the use of functional permanent materials, which exhibit an application-specific refractive index [4]. Additionally, substrate preparation for quantum dot growth is an interesting and relevant application

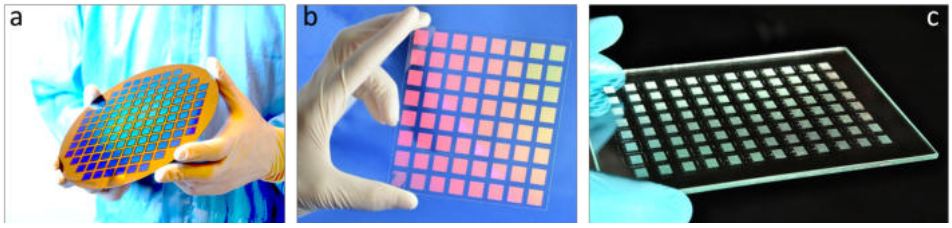


Figure 2: a,b step & repeat NIL for nanoscale features (imprint material mr-NIL212 FC from micro resist technology), c step & repeat for microstructures (OrmoClear from micro resist technology).

[5]. Figure 3 shows PICs (photonic integrated circuits), which were fabricated for LiDAR applications [6]. The poster will present additional application scenarios for NIL.

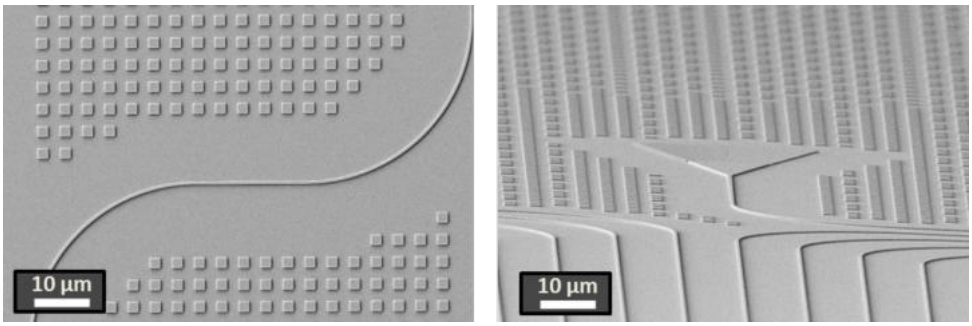


Figure 3: Top view SEM images of imprinted waveguide test structures imprinted in a high refractive index resin (IPO912, Inkron) [6]

Acknowledgements

The authors acknowledge funding from Austrian and European projects, especially the Lampion project (FFG 861414), the M3dRES project (FFG 858060), as well as the TINKER (EU H2020 958472) and E2PACKMAN projects (Chips JU 101194187).

Summary

In summary, nanoimprint lithography is a very versatile technique with a broad application potential. We would like to contribute with our NIL technologies to address the needs of the quantum technologies community.

References

[1] Michael Mühlberger, editor. *Nanoimprint Lithography Technology and Applications*. MDPI-Multidisciplinary Digital Publishing Institute, 2022.

[2] Amiya R Moharana, Helene M Außerhuber, Tina Mitteramskogler, Michael J Haslinger, and Michael M Mühlberger. Multilayer nanoimprinting to create hierarchical stamp masters for nanoimprinting of optical micro-and nanostructures. *Coatings*, 10(3):301, 2020.

[3] S Kopp, V Jonaityte, MJ Haslinger, and MM Mühlberger. A step and repeat and roll-to-plate nanoimprint process for the fabrication of nanostructured substrates. In *40th European Mask and Lithography Conference (EMLC 2025)*, volume 13787, pages 242–249. SPIE, 2025.

[4] Michael J Haslinger, Sonja Kopp, Voktorija Jonaityte, Amiya Moharana, Helene Außerhuber, and Michael M Mühlberger. Direct patterning of functional materials using nanoimprint lithography. In *38th European Mask and Lithography Conference (EMLC 2023)*, volume 12802, pages 249–257. SPIE, 2023.

[5] E Lausecker, M Brehm, M Grydlik, F Hackl, I Bergmair, M Mühlberger, T Fromherz, F Schäffler, and G Bauer. Uv nanoimprint lithography for the realization of large-area ordered sige/si (001) island arrays. *Applied Physics Letters*, 98(14), 2011.

[6] Jerome Reche, Michael Haslinger, Martin Eibelhuber, Mikko Poutanen, and Kazuki Origuchi. High potential of nanoimprint lithography for lidar application. In *39th European Mask and Lithography Conference (EMLC 2024)*, volume 13273, pages 166–171. SPIE, 2024.

Enhancing Light-Matter Interactions In Integrated Platforms

Malaika Waheed[1,2], Sarah M. Skoff[1], Christian Koller[2]

[1]Atominstitut, TU Wien, 1020 Wien, Austria

[2]Fachhochshule Wiener Neustadt, University of Applied Sciences, Austria

sarah.skoff@tuwien.ac.at

Abstract

The two-dimensional van der Waals materials, such as hexagonal boron nitride, represent a versatile platform for quantum sensing at room temperature. The defects in hBN offer the properties of emitting single photons. These single photon emitters are of more interest as they offer optically detectable spin resonances under a controlled environment. Thus, our work proposes the study of optically detectable magnetic resonances of these defects in hBN. For the microwave control and spin readout of these defects, the design and characterization of an on-chip CMOS-compatible module is important to implement, which is an ideal miniaturized solution for bulky systems. With on-chip design and ODMR analysis of point defects in hBN, this work will potentially contribute towards scalable, high-performance solutions for quantum photonics and sensing applications.

Introduction and Background

The optically addressable spin defects in hBN represent a novel platform for nanoscale quantum sensing, wherein the atomic thickness and layered characteristics of the host material may facilitate enhanced spatial resolution and create new prospects for combination with integrated systems [1]. 2D hBN defects produce bright and stable single photon emitters (SPEs) at room temperature. Hence, unlike many quantum emitters that require cryogenic conditions, hBN demonstrates bright and optically stable single photon emission at room temperature, making it highly practical for real-world quantum technology and sensing applications. For all of that to work, traditional sensors require bulky components, including a mounted laser, power supply, microwave generator, conductors to route the microwaves, and single photon detector.

Methods / Experiment

For the optical characterisation of hBN, the custom-built confocal microscope used shown in Figure 1 [2]. With the addition of microwave delivery structure we can make it detect ODMR signals. For the microwave control and spin readout, we propose the On-Chip solution based on inexpensive components using standard complementary metal-oxide-semiconductor (CMOS) technology. So this is a compact alternative to traditional bulky components. The schematic of the proposed on-chip system is shown in Figure 2. For the chip fabrication, the top-level architecture is designed first and then tested with Cadence.

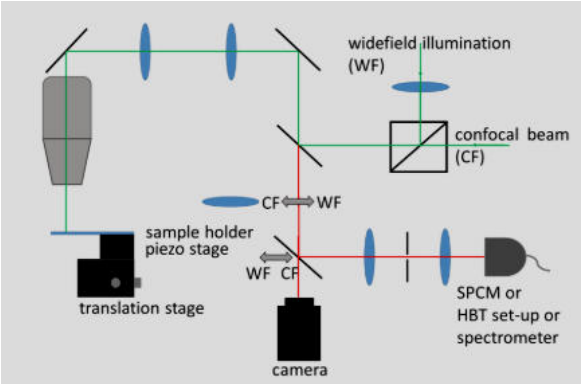


Figure 1: Schematic of custom-built confocal microscope for characterising quantum emitters in hBN [2].

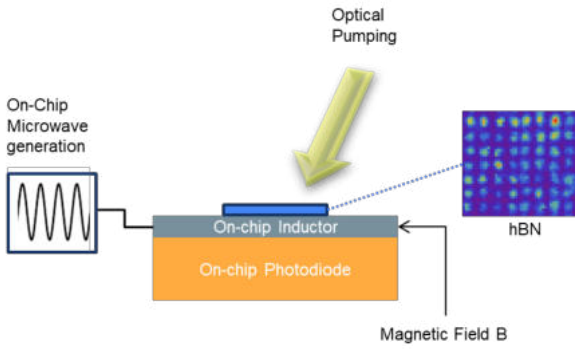


Figure 2: Schematic of On-Chip system

Results and Discussion

With our custom-built microscope, hBN samples are investigated, below you see an example of a trilayer hBN sample in Figure 3 and Figure 4 [2] and of an exfoliated sample with emission sites fabricated at specific locations by ion bombardment in Figure 5. The collected fluorescence is sent to a Hanbury-Brown–Twiss (HBT) setup to verify single-photon emission or to a spectrometer to evaluate the photoluminescence spectrum shown in Figure 4. In Figure 5, we perform confocal imaging to collect fluorescence and reflection signals from the sample prepared by exfoliation and the ion bombardment technique to have boron vacancy defects in hBN.

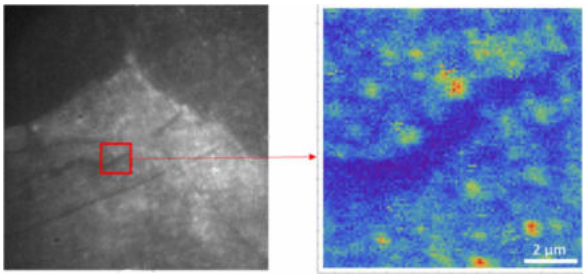


Figure 3: WideField imaging (Left) and confocal imaging (Right) of trilayer engineered hBN sample.

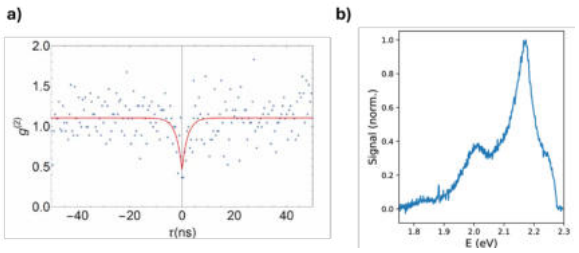


Figure 4: a) Second order intensity correlation measurements. b)PL spectra of defects found in CVD-grown, layer-engineered hBN

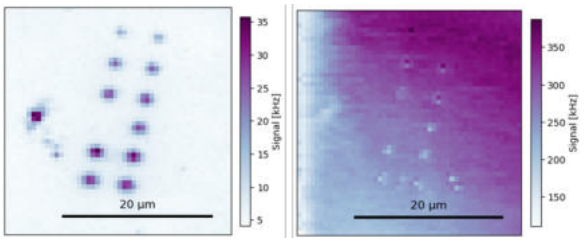


Figure 5: Confocal imaging of VB- ensembles [Sample fabrication from group of Prof. A. Kumar, IIT Bombay; A. Majumder and Dr. K. Bera]

A universal integrated optical sensor is shown in Figure 6 for the detection, amplification and digitalization of various optical data signals.

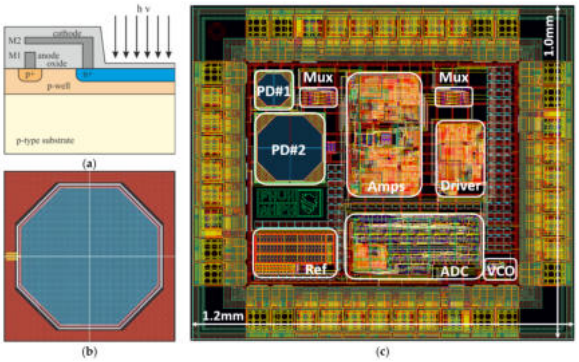


Figure 6: Integrated Optical Sensor (**a**) photodiode cross section, (**b**) photodiode layout and (**c**) complete chip layout with highlighted functional blocks [3]

References

[1] Sam C Scholten, Priya Singh, Alexander J Healey, Islay O Robertson, Galya Haim, Cheng Tan, David A Broadway, Lan Wang, Hiroshi Abe, Takeshi Ohshima, et al. Multi-species optically addressable spin defects in a van der waals material. *Nature Communications*, 15(1):6727, 2024.

[2] Ambika Shorny, Hardy Schauffert, James C Stewart, Sajid Ali, Stefan Walser, Helmut Hörner, Adarsh S Prasad, Vitaly Babenko, Ye Fan, Dominik Eder, et al. Properties of quantum emitters in different hbn sample types particularly suited for nanophotonic integration. *Materials for Quantum Technology*, 5(2): 025401, 2025.

[3] Alexander Nemecek, Philipp Neumann, and Christian Koller. Universal integrated photodetector platform. *Proceedings*, 2(13), 2018. ISSN 2504-3900. doi: 10.3390/proceedings2130756. URL `https://www.mdpi.com/2504-3900/2/13/756`.

System-Level Optimization of NV$^-$-Diamond-Based Gyroscopes using Pymond

Matthäus Hirsch[1,2], Enrique Sánchez-Ibáñez[1], Claudius Mullen[1], Matthijs Wanrooij[1] Mario Grüneberg[1], Tilen Knaflič[1], Jaka Pribošek[1]

[1]Applied Quantum Sensing Group, Silicon Austria Labs, Villach, Austria

[2]Walter Schottky Institut and Physik-Department, Technical University of Munich, Munich, Germany

matthaeus.hirsch@silicon-austria.com / m.hirsch@tum.de

Abstract

The development of solid-state-defect-based quantum devices lacks accurate simulation-based techniques for system-level parameter optimization. Here, a method is presented to optimize three key system-parameters of NV$^-$-diamond-based gyroscopes (excitation beam waist, antenna diameter, and confocal filtering pinhole diameter) for maximum signal to noise ratio (SNR). Using `Pymond`, a python package for spatially resolved simulations of solid-state-defects, the parameter space was sampled using 1700 simulation runs (10x17x10 grid). In each run the gyroscopic sensing protocol was carried out on ∼5000 spatial points inside the diamond, accounting for distinct local RF and optical excitation profiles dictated by antenna and laser parameters. The resulting spin-dependent fluorescence was propagated through the optical collection path for signal calculation. This method revealed a global maximum of the SNR, identifying the optimal parameter set for peak sensor performance. Our results demonstrate a scalable, simulation-first design framework that accelerates quantum sensor development and reduces experimental trial-and-error.

Introduction and Background

Solid-state defect platforms for quantum sensing offer great potential, yet systematic, simulation-driven optimization of device-level parameters remains challenging. Among emerging quantum sensors, NV$^-$-center-based gyroscopes have attracted significant interest. As demonstrated by Jarmola et al.[1] rotation can be transduced into spin-state modulations through the application of a double-quantum nuclear 4-Ramsey protocol, which can be measured by fluorescence detection. The performance of these devices is strongly governed by the interplay between optical excitation, RF driving fields, and detection geometry. In particular, parameters such as the excitation beam waist and the RF antenna dimensions critically determine the inhomogeneities the spin-ensemble experiences during a measurement run, while the size of the pinhole used for confocal filtering selects the origin and amount of fluorescence collected as signal. Without a unified computational framework, identifying the optimal parameter combination requires extensive experimental trial-and-error, limiting performance scaling.

Simulation Methods

To address this gap, we employ `Pymond`, a Python-based simulation toolkit designed for spatially resolved modeling of solid-state defect systems, particularly developed for NV$^-$-diamond applications. `Pymond` enables efficient computation of the behavior of spatially distributed NV$^-$-ensembles in position-dependent non-homogeneous fields (laser excitation and RF-driving).[2]

The goal was to find an optimal parameter set for three of the main experimental parameters, excitation beam waist, RF antenna diameter, and confocal pinhole size. An approach was chosen where first, the fluorescence produced by the spatially distributed NV$^-$-ensemble was simulated as a function of excitation beam waist and RF antenna diameter. Second, the fluorescence signal reaching the detector, influenced by the pinhole size, was calculated for each parameter set.

For the parameter-optimization 10 different laser fields, approximated as Gaussian beams with varying beam waists at the focus point, and 17 different RF antenna fields, simulated using antenna geometry with the `Python` library `magpylib`, were prepared. Subsequently these were combined into 170 unique simulation runs in `Pymond`. In each run a double-quantum nuclear 4-Ramsey protocol was carried out on a 21x21x11 grid of spatially distributed NV$^-$-centers using the given driving fields. To extract the rotation-dependent signal, the protocol was executed under two conditions: (i) with the diamond rotating at 1 Hz, and (ii) with the diamond stationary. The final gyroscopic readout was computed as the differential fluorescence between these two measurements.

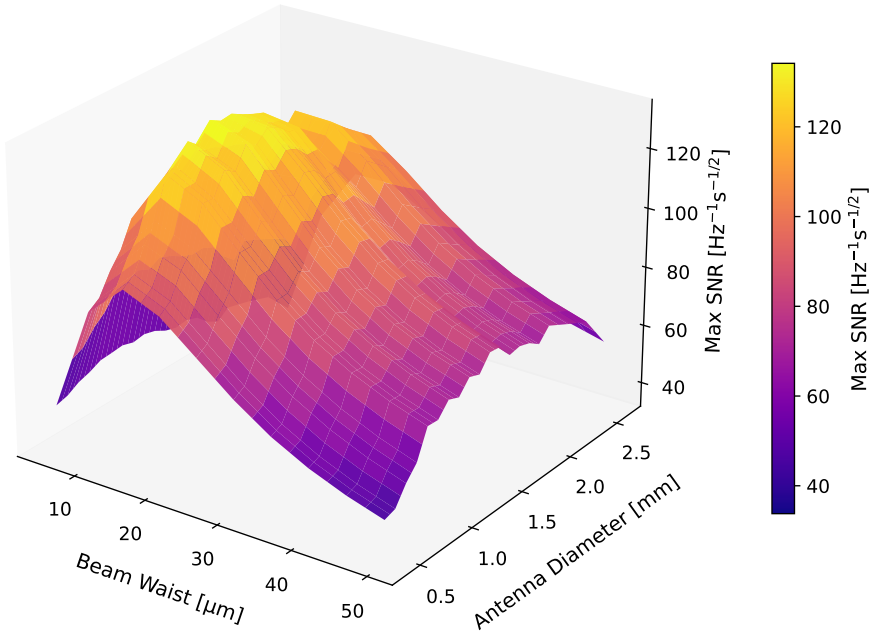


Figure 1: Simulated shot-noise limited signal-to-noise ratio (SNR) response surface for the NV$^-$-diamond gyroscope. The vertical axis represents the maximum achievable SNR, plotted as a function of the excitation beam waist (x-axis) and RF antenna diameter (y-axis). Each marker on the surface corresponds to the peak SNR obtained after optimizing the confocal pinhole diameter for that specific beam-antenna combination. The global maximum identifies the system-level parameter set that maximizes gyroscopic sensitivity.

The fluorescence profiles resulting from the simulation runs were stored for every NV$^-$-center of the spatially distributed ensemble. Subsequently, for each of the runs 10 different collection systems with varying pinhole diameter were applied, and the resulting signal reaching the detector was recorded. Using this detector signal, the shot-noise limited SNR of the rotation measurement, the main figure of merit for this study, was calculated. Figure 1 maps the resulting parameter space, showing the maximum achievable SNR as a function of beam waist and antenna diameter, with the confocal pinhole diameter pre-optimized at each coordinate.

Results and Discussion

Figure 1 reveals strong interdependence of the experimental parameters and highlights the importance of optimization for SNR maximization. A variation of the SNR of a factor 3 is observed in the relevant parameter space. One global SNR peak arises at an excitation beam waist of 15 µm, an RF antenna diameter of 1.2 mm and a pinhole size of 75 µm (5 $*$ beam waist). While our model assumes ideal Gaussian beam profiles and neglects dynamic noise sources, it establishes a deterministic design workflow that directly informs laser focusing, antenna fabrication, and pinhole selection. Future work will validate these parameters experimentally. Overall, this simulation-first framework replaces trial-and-error tuning with predictive optimization, accelerating NV$^-$-center gyroscope development and providing a scalable design tool for solid-state quantum sensors.

Acknowledgments

This work was supported by the FFG Project MAGELLAN (Nr.929206) as well as the MSCA Crystalline, HORIZON-MSCA-2022-COFUND-01-01, Grant No. 101126571.

References

[1] Andrey Jarmola, Sean Lourette, Victor M. Acosta, A. Glen Birdwell, Peter Blümler, Dmitry Budker, Tony Ivanov, and Vladimir S. Malinovsky. Demonstration of diamond nuclear spin gyroscope. *Science Advances*, 7(43), October 2021. ISSN 2375-2548. doi: 10.1126/sciadv.abl3840. URL `http://dx.doi.org/10.1126/sciadv.abl3840`.

[2] Enrique Sánchez-Ibáñez et al. Pymond: a package for system-level simulation of nv– center-based technologies. (in preparation).

Sensing and Quantum Sensing with Light-Matter Interaction

Markus Weber[1], Josef Resl[1], Andreas Supersperger[1], David Jakob[1], Hideaki Takashima[2], Andreas W. Schell[1]

[1]Division of Light-Matter Interaction, Johannes Kepler University, Linz, Austria

[2]Chitose Institute of Science and Technology, Hokkaido, Japan

corresponding author: markus.weber@jku.at

Abstract

Optical light-matter interaction drives a vast array of innovative sensing applications, pushing the boundaries of industrial technological advancement. This overview highlights our ongoing research at the intersection of fundamental science and industrial application. Specifically, we present recent progress in: (a) high-sensitivity magnetic field measurements using electromagnetically induced transparency (EIT) in room-temperature alkali vapors; (b) the identification of levitated charged nanoparticles via optical Raman spectroscopy in a Paul trap; and (c) the fabrication of Bragg gratings on evanescent optical field sensors using nanoimprint lithography (NIL).

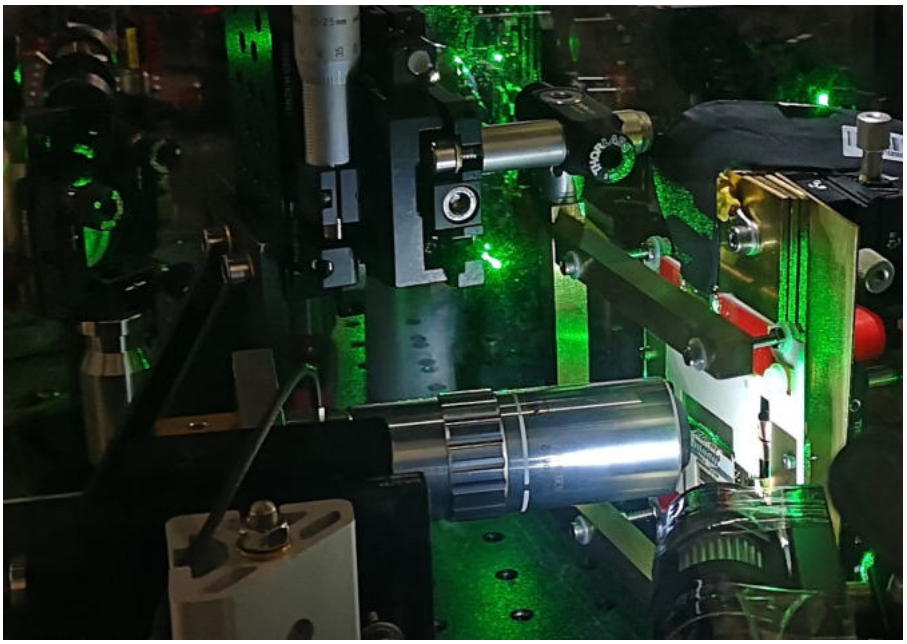


Figure 1: Photograph of our Paul trap, which enables the investigation of the optical properties of levitated nanoparticles via in-situ Raman microscopy.

Pymond: a package for system level optimization of solid-state spin based devices

Enrique Sánchez-Ibáñez, Matthijs Wanrooij, Mario Grüneberg, Matthäus Hirsch, Tilen Knaflič, Claudius Mullen, Jaka Pribošek

Applied Quantum Sensing, Silicon Austria Labs, Europastraße 12, 9524 Villach, Austria

enrique.sanchez@silicon-austria.com

Abstract

The estimation of the performance of solid-state-defect-based quantum devices lacks a system-level approach beyond the performance of an ideal single point. In this work, we present the Python package `Pymond`, aimed at providing fast, system level spin dynamics simulations, tailored for simulating realistic quantum devices employing nitrogen-vacancy (NV) centers in diamond. Pymond, however, features a modular structure and thus allows straightforward extension to other solid-state-defect-based technologies. Our approach relies on semi-analytical approximation, widely valid under typical conditions in quantum control. This opens a faster alternative to computationally heavy numerical methods, enabling system-level optimization of quantum control protocols and device design, essential for both academic research and development of real industrial applications.

Introduction

Quantum sensing with diamond has gained traction over the last decade as an outstanding platform for quantum technologies. The nitrogen vacancy (NV) center in diamond, which is created by replacing two adjacent carbon atoms in the lattice by a nitrogen atom and a vacancy, has proven particularly interesting because it allows all-optical initialization and readout of electron and nuclear spins at room temperature. `Pymond` is an open-source, system level simulation tool for the nitrogen vacancy center in diamond that can handle both ideal, single-point NV's as well as large sampling volumes [1]. While other open-source libraries, such as `QuTip`, `SimOS` and `QuaCCAToo`, incorporate functionality for NV sensing and offer strong performance with regard to accuracy, their implementation is fully numerical and therefore computationally expensive. `Pymond`, on the other hand, combines analytical formulations with numerical optimization to build a semi-analytic approach that can reduce computational cost by orders of magnitude.

Structure of the package

The structure of `Pymond` is illustrated in Figure 1 (left). `Pymond` features strong performance in the following domains:

- The package is designed to decouple inherent properties of the defect (Hamiltonian, Lindblad operators, etc.) from quantum control methods to allow for straightforward expansion to additional defects containing other nuclear spins than ^{14}N.
- The package supports user-defined input fields (e.g. magnetic field and temperature), custom quantum control sequences (via AC magnetic field pulses) and optical driving, as well as uncomplicated transitioning between the lab frame and the defect frame.
- By making the valid assumption that open-system dynamics takes places on much longer timescales than the duration of RF pulses and assuming weak driving to justify the rotating wave approximation, `Pymond` manages to drastically speed up simulations using a semi-analytical framework, instead of relying on a fully numerical approach.
- By exploiting the fact that many subspaces of the Liouvillian superoperator $\mathcal{L}$ are either situationally or permanently decoupled, `Pymond` can reduce its dimension by building and condensing a directed graph of $\mathcal{L}$ followed by topological ordering, further reducing computational cost by up to orders of magnitude.
- `Pymond` supports both single NV's as well as large sensing volumes, with built-in methods to generate and apply custom scalar and vector fields throughout the sensing volume.

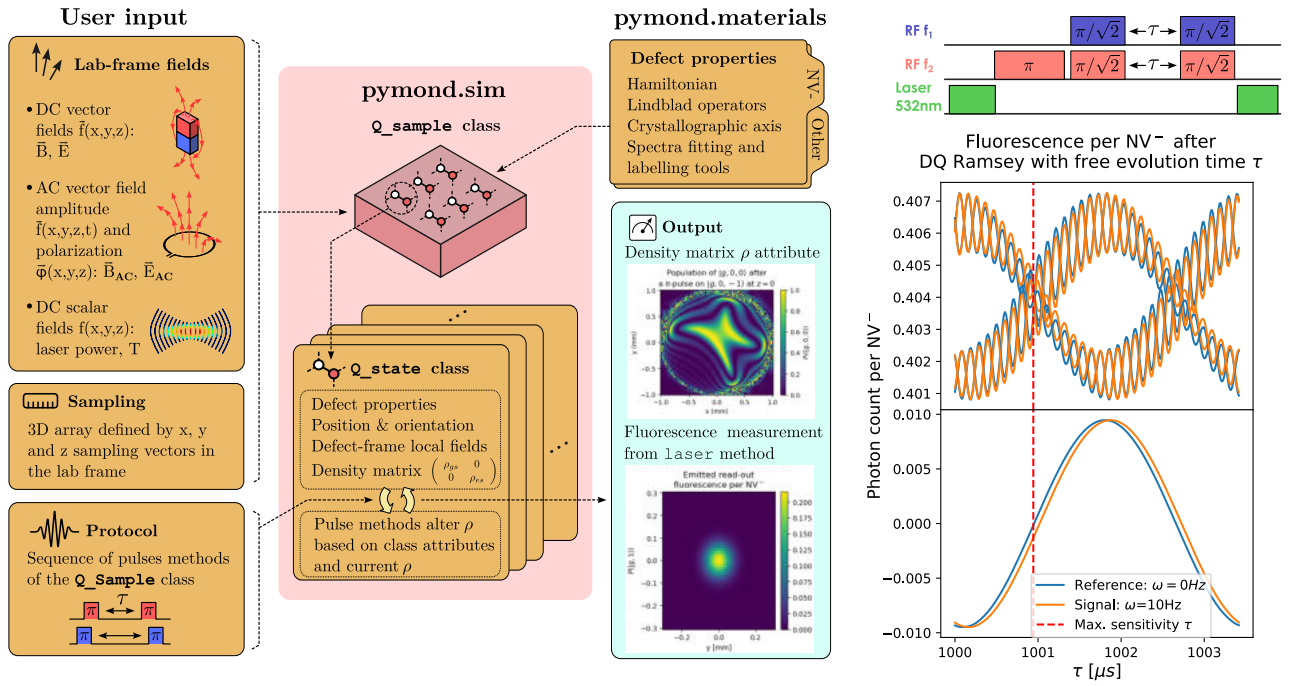


Figure 1: (left) Summary of the module structure and flow of data of the `Pymond` package. (right) A 4-DQ Ramsey pulse sequence and its simulation in `Pymond`. The top panel shows a schematic of the pulse sequence. The middle panel shows simulated photon count per NV^- as a function of free precession time τ, for each of 4 fringes which differ by relative phase shifts in the last two-tone $\pi/\sqrt{2}$ pulse. The signal is taken at a rotation rate of 10 Hz around the quantization axis, while the reference represents a stationary measurement. The bottom panel shows the result of combining the fringes to eliminate single quantum transitions.

Example use case

To demonstrate the usefulness and predictive power of `Pymond`, we simulate a full 4-DQ Ramsey protocol [2] aimed at quantum gyroscopy, see Figure 1 (right). The signal is taken at a rotation rate of 10 Hz around the quantization axis, while the reference is recorded in the absence of rotation. The protocol features hyperpolarization of the nuclear spin to $|g,0,1\rangle$ using the Excited State Level Anticrossing (ESLAC) technique, which relies on a static magnetic field of approximately 50 mT to transfer electronic spin polarization to the nuclear spin. The nuclear spin is then driven to $|g,0,0\rangle$. Subsequently, a two-tone Ramsey sequence is performed on the $|g,0\rangle$ triplet. Full-sample fluorescence shows a combination of $f_1 - f_2$ and f_1 and f_2, of which the last two are detrimental to rotation sensing and can be suppressed by a linear combination of the fluorescence obtained with four complementary phases in the last coherent pulse of the sequence, resulting in the smooth fringes of the bottom panel. The red line marks the point of maximum sensitivity to rotation measurement, see the supplementary materials of [2].

Acknowledgments

This work was supported by the FFG Projects GIRAFFE (Nr.900373) and MAGELLAN (Nr.929206) as well as the MSCA Crystalline, HORIZON-MSCA-2022-COFUND-01-01, Grant No. 101126571.

References

[1] Sánchez-Ibáñez, E. et al. *Pymond: a package for system-level simulation of NV⁻ center-based technologies* (in preparation).

[2] Jarmola, A. et al. *Demonstration of diamond nuclear spin gyroscope*. Sci. Adv. 7, eabl3840 (2021).

Sensitivity-enhanced mid-IR OCT with undetected photons for additive ceramic manufacturing

Michela Conti[1], Paul Gattinger[1], Andreas W. Schell[2], and Ivan Zorin[1]

[1]RECENDT – Research Center for Non-Destructive Testing, Linz, Austria
[2]Institute of Semiconductor and Solid State Physics, Johannes Kepler University, Linz, Austria
michela.conti@recendt.at

Abstract

Mid-infrared (mid-IR) optical coherence tomography (OCT) enables volumetric non-destructive inspection of additively manufactured ceramics by exploiting the strong reduction of light scattering at wavelengths of 3 - 4 μm, achieving 80 dB sensitivity and 8 μm axial resolution. A quantum alternative based on nonlinear interferometry with entangled photon pairs allows mid-IR imaging using only near-IR room-temperature detectors, but currently reaches only 69 dB sensitivity. This work proposes to bridge this gap through a monolithic pump-enhanced entangled photon source, in which a pump-resonant cavity around the nonlinear crystal boosts the pair generation rate by a factor N (number of round trips), thus enhancing the signal-to-noise ratio by $\sqrt{N}$ in the shot-noise-limited regime.

Introduction and Background

Additive ceramic manufacturing (ACM) has rapidly expanded across biomedicine, microelectronics, and industrial engineering, producing complex parts from materials such as alumina and zirconia.

Optical coherence tomography (OCT) is a contactless, non-destructive high-resolution (micrometer-scale) 3D imaging technique that reconstructs sub-surface structure from backscattered light. OCT does not require sample preparation as opposed to alternative techniques. Standard OCT systems operate in the near-infrared (800 - 1300 nm), where ceramic materials exhibit strong elastic light scattering that limits penetration to only a few micrometers.

As scattering scales with the inverse fourth power of wavelength, shifting to the mid-IR (3 - 4 μm) reduces this limitation, enabling volumetric imaging up to ∼1 mm (and beyond) deep in porous ceramics [1]. Classical mid-IR OCT has been demonstrated on 3D-printed alumina and zirconia, resolving sub-surface defects, individual printed layers, porosity gradients, and multi-material interfaces with 8 μm axial resolution and ∼80 dB system sensitivity [1]. This performance is entirely inaccessible to commercial near-IR OCT systems, as shown in Fig. 1.

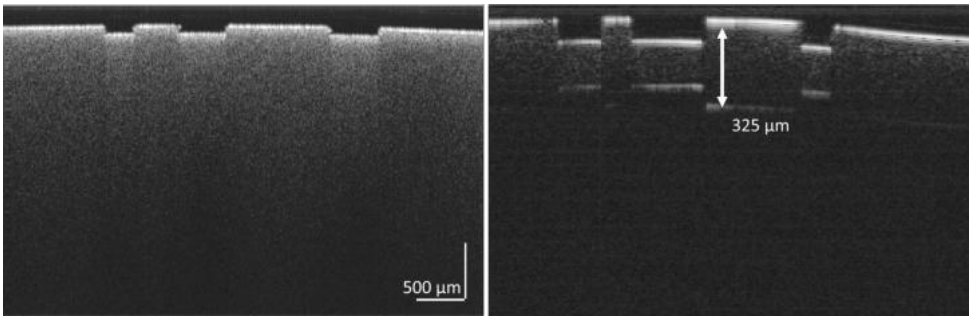


Figure 1: OCT images of a lithography-based ceramics manufactured (LCM) part with high porosity of 4.59% obtained with: (left), standard OCT at 1300 nm; (right), quantum-based OCT with undetected photons at 3780 nm.

Despite its imaging capabilities, classical mid-IR OCT faces a significant barrier to industrial adoption: broadband mid-IR sources and detectors are expensive, exhibit limited performance and are technically demanding. A quantum approach based on nonlinear interferometry offers a route around this [2]. Entangled photon pairs are generated via spontaneous parametric down-conversion (SPDC): mid-IR idler photons probe the sample, while their near-IR signal partners are detected on a standard room-temperature silicon spectrometer, making mid-IR sources and detectors obsolete. Operating in the shot-noise limit, the technique possesses only sub-nW

probe powers, which might be critical for green ceramic parts where polymer binders absorb mid-IR radiation and risk thermal damage or polymerization under classical illumination. Quantum mid-IR OCT has been demonstrated with 10 μm axial resolution on thick alumina structures, but achieves only 69 dB sensitivity [3], below the classical 80 dB benchmark, due to the limited brightness of SPDC sources [4].

Experiment

The quantum-based OCT (with undetected photons) system is based on a nonlinear interferometer with Michelson topology. A visible pump laser (660 $\sim$ nm) drives SPDC in a nonlinear crystal, generating entangled photon pairs with idler photons in the mid-IR range (3.3 - 4.3 μm) and signal photons in the near-IR domain ($\sim$800 nm). The idler photons probe the ceramic sample; the signal photons, after a double pass in the non linear crystal, are detected by a silicon spectrometer, as shown in Fig. 2. A Fourier-domain OCT post-processing protocol of the measured signal spectral interferograms yields the depth-resolved reflectivity profile of the sample, entirely analogously to classical frequency-domain OCT, but without any mid-IR component or source in the detection chain.

The central innovation of this project is the introduction of a monolithic pump-resonant cavity directly enclosing the nonlinear crystal. Due to multiple round trip of the pump beam through the nonlinear crystal, the effective SPDC pair-generation probability is enhanced, and thus the detected photon flux by a factor N. The cavity is designed as a fully monolithic platform; the corresponding OCT system with such an integrated source is shown schematically in Fig.3.

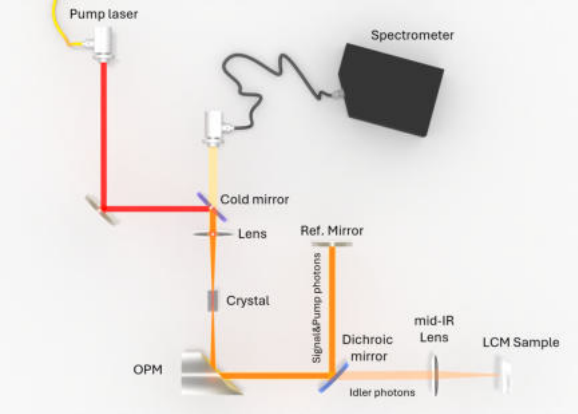


Figure 2: Quantum-based OCT with undetected photons setup

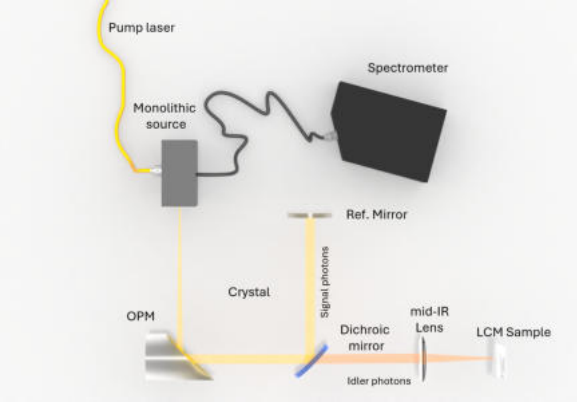


Figure 3: Sensitivity-enhanced quantum-based OCT with undetected photons

Expected Results

Since the system operates in the shot-noise limit, the signal-to-noise ratio scales as the square root of the number of detected photons. Enhancing the photon flux by a factor N through the pump cavity therefore yields a direct improvement of the SNR by:

$$\mathrm{SNR}_{\mathrm{enh}} = \sqrt{N}\,\mathrm{SNR}_{\mathrm{dp}}, \tag{1}$$

as compared to the standard double-pass (dp) scheme.

This enhancement is expected to be sufficient to bridge, and potentially surpass, the gap between the demonstrated 69 dB quantum sensitivity and the 80 dB classical benchmark. This would make quantum mid-IR OCT competitive with classical systems in sensitivity terms, while retaining the full advantages of near-IR detection. The successful demonstration of this architecture would establish quantum nonlinear interferometry as a practically viable platform for industrial non-destructive testing, opening perspectives beyond ceramics to pharmaceutical coatings, composite materials, and cultural heritage conservation.

Funding

This project is co-financed by research subsidies granted by the government of Upper Austria: Quick (Wi-2022-597365/18-Au) and FTI 2025 (EQUAMP, 2025-213468/12-FrJ). The authors acknowledge funding and support from Österreichische Forschungsförderungsgesellschaft (FFG) under QMIRACT Project (929209).

References

[1] Ivan Zorin, Dominik Brouczek, Sebastian Geier, Serkan Nohut, Julia Eichelseder, Guillaume Huss, Martin Schwentenwein, and Bettina Heise. Mid-infrared optical coherence tomography as a method for inspection and quality assurance in ceramics additive manufacturing. *Open Ceramics*, 12:100311, 2022. ISSN 2666-5395. doi: https://doi.org/10.1016/j.oceram.2022.100311.

[2] Gabriela Barreto Lemos, Victoria Borish, Garrett D. Cole, Sven Ramelow, Radek Lapkiewicz, and Anton Zeilinger. Quantum imaging with undetected photons. *Nature*, 512(7515):409–412, August 2014. ISSN 0028-0836, 1476-4687. doi: 10.1038/nature13586.

[3] Aron Vanselow, Paul Kaufmann, Ivan Zorin, Bettina Heise, Helen M. Chrzanowski, and Sven Ramelow. Frequency-domain optical coherence tomography with undetected mid-infrared photons. *Optica*, 7(12): 1729–1736, Dec 2020. doi: 10.1364/OPTICA.400128.

[4] Paul Gattinger, Andreas W. Schell, Sven Ramelow, Markus Brandstetter, and Ivan Zorin. Quantum fourier transform infrared spectroscopy: Evaluation, benchmarking, and prospects. *Applied Spectroscopy*, 79(12): 1737–1746, 2025. doi: 10.1177/00037028251340945.

Organizers & Partners

QSL26 is organized by RECENDT and JKU Linz with the support of its partners. The organizers gratefully acknowledge the contributions of all speakers, poster presenters, participants, and supporting institutions.

Organizers

RECENDT
RESEARCH CENTER NON DESTRUCTIVE TESTING

JKU
JOHANNES KEPLER UNIVERSITY LINZ

Supported by

FFG
Forschung wirkt.

ober österreich

Partners & Networks

MC
MECHATRONIK CLUSTER

business upper austria

Member of UAR INNOVATION NETWORK

PHOTONICS AUSTRIA

#QSL26

Conference Proceedings

https://www.recendt.at
office@recendt.at

